

DETERMINE THE GALAXY BIAS FACTORS ON LARGE SCALES USING BISPECTRUM METHOD

H. GUO^{1,2}, Y. P. JING¹*Draft version July 2, 2009*

ABSTRACT

We study whether the bias factors of galaxies can be unbiasedly recovered from their power spectra and bispectra. We use a set of numerical N -body simulations and construct large mock galaxy catalogs based upon the semi-analytical model of Croton et al. (2006). We measure the reduced bispectra for galaxies of different luminosity, and determine the linear and first nonlinear bias factors from their bispectra. We find that on large scales down to that of the wavenumber $k = 0.1 h\text{Mpc}^{-1}$, the bias factors b_1 and b_2 are nearly constant, and b_1 obtained with the bispectrum method agrees very well with the expected value. The nonlinear bias factor b_2 is negative, except for the most luminous galaxies with $M_r < -23$ which have a positive b_2 . The behavior of b_2 of galaxies is consistent with the b_2 mass dependence of their host halos. We show that it is essential to have an accurate estimation of the dark matter bispectrum in order to have an unbiased measurement of b_1 and b_2 . We also test the analytical approach of incorporating halo occupation distribution to model the galaxy power spectrum and bispectrum. The halo model predictions do not fit the simulation results well on the precision requirement of current cosmological studies.

Subject headings: gravitational lensing—dark matter— cosmology: theory— galaxies: formation

1. INTRODUCTION

In the current Λ CDM cosmological scenario, dark matter dominates the matter density in the universe, and luminous galaxies are thought to be formed within dark matter halos. However, detailed physical processes of galaxy formation, such as star formation and supernova feedback, are very complicated. Different prescriptions of galaxy formation may lead to different relations between luminous galaxies and the underlying dark matter, or equivalently, different galaxy biases (e.g., Kaiser 1984; Davis et al. 1985; Bardeen et al. 1986). Therefore, the key to our understanding of galaxy formation is to study the galaxy bias both in theories and observations. If galaxy formation is mainly determined by local physical processes (such as hydrodynamics), the galaxy bias is then a constant on large scales (Coles 1993). In the first order, the galaxy density fluctuation is proportional to that of the dark matter on large scales, $\delta_g \propto \delta_m$. The coefficient here is usually called as the linear bias factor, b_1 . It is important to study its dependence on the luminosity, morphology, mass, and redshift of galaxies (e.g., Xia et al. 1987; Börner et al. 1991; Norberg et al. 2002; Jing et al. 2002; Zehavi et al. 2004; Park et al. 2005; Li et al. 2006; Meneux et al. 2008), because this information provides important clues to how galaxies are formed.

The bias factor b_1 and its relation with the scale k can be determined directly from the ratios between the power spectra of galaxies ($P_g(k)$) and those of the underlying dark matter ($P_m(k)$),

$$P_g(k) = b_1^2(k)P_m(k), \quad (1)$$

where the higher-order terms are negligible. But it is

important to note that the power spectrum of dark matter is usually not known in observations. Therefore, the absolute value of $b_1(k)$ cannot be obtained through the above relation, unless the power spectrum of dark matter is measured from observations, such as future weak lensing surveys. From Equation (1), we note that the bias factor b_1 actually couples with the properties of the large-scale matter density field, such as the linear rms fluctuation, σ_8 . And it is impossible to break such degeneracy only by using the galaxy power spectrum. It is then challenging to determine the galaxy bias purely in observations.

Fortunately, there is a way of doing this by involving the second-order statistics, the bispectrum $B(k_1, k_2, k_3)$, or more conveniently the reduced bispectrum $Q(k_1, k_2, k_3)$, which is defined by

$$Q(k_1, k_2, k_3) = \frac{B(k_1, k_2, k_3)}{P(k_1)P(k_2) + cyc}, \quad (2)$$

where (k_1, k_2, k_3) are the three sides of a triangle and $P(k)$ is the corresponding power spectrum (galaxy or dark matter). On sufficiently large scales where the density fluctuation is small, we can expand the galaxy density field δ_g in the Taylor series of δ_m , which up to the second order can be written as

$$\delta_g = b_1\delta_m + \frac{1}{2}b_2\delta_m^2, \quad (3)$$

where b_1 is the linear bias factor and b_2 is the first nonlinear bias factor. If we assume that the bias factors are deterministic, i.e., constant b_1 and b_2 , we can derive the following relation from Equation (3) by utilizing the reduced bispectra Q_g of galaxies and Q_m of dark matter (e.g., Fry 1994; Gaztanaga & Frieman 1994; Mo, Jing & White 1997),

$$Q_g(k_1, k_2, k_3) = \frac{Q_m(k_1, k_2, k_3)}{b_1} + \frac{b_2}{b_1^2}. \quad (4)$$

¹ Key Laboratory for Research in Galaxies and Cosmology, Shanghai Astronomical Observatory, Chinese Academy of Sciences, Nandan Road 80, Shanghai 200030, China; guoh@shao.ac.cn, ypjing@shao.ac.cn.

² Graduate School of the Chinese Academy of Sciences, 19A, Yuquan Road, Beijing, China

According to the second-order perturbation theory, the reduced bispectrum of dark matter $Q_m(k_1, k_2, k_3)$ can be predicted on large scales based on the measurement of galaxy power spectrum. In the second-order perturbation theory (hereafter PT2), it gives (Fry 1984; Matarrese et al. 1997; Bernardeau et al. 2002)

$$B_{PT}(k_1, k_2, k_3) = F(\mathbf{k}_1, \mathbf{k}_2) P_L(k_1) P_L(k_2) + cyc \quad (5)$$

$$F(\mathbf{k}_1, \mathbf{k}_2) = (1 + \mu) + \frac{\mathbf{k}_1 \cdot \mathbf{k}_2}{k_1 k_2} \left(\frac{k_1}{k_2} + \frac{k_2}{k_1} \right) + (1 - \mu) \left(\frac{\mathbf{k}_1 \cdot \mathbf{k}_2}{k_1 k_2} \right)^2, \quad (6)$$

where $\mu = 3\Omega_m^{-2/63}/7$ denotes the mild dependence on cosmology and $P_L(k)$ is the linear dark matter power spectrum. It is easy to see that within the tree-level PT, the reduced bispectrum $Q_m(k_1, k_2, k_3)$ does not depend on redshift or amplitude of the matter density fluctuation, but weakly depends on the cosmology, thus depends almost solely on the shape of the matter power spectrum. Therefore, the reduced bispectrum $Q_m(k_1, k_2, k_3)$, on large scales, can be predicted from the measurement of galaxy power spectrum, since the galaxy power spectrum $P_g(k)$ has the same shape as the matter power spectrum $P_m(k)$ (they are proportional to each other on large scales). The bias factors b_1 and b_2 can then be determined from the measurement of Q_g and the prediction of Q_m , with at least two independent triangle configurations from the galaxy distribution. Many more configurations are actually used in the real measurement, because the measurement errors are present. With the value of b_1 , one can determine the amplitude of the linear density fluctuation from the galaxy distribution alone, which can thus become a potentially powerful way for dark energy study if the density fluctuation amplitude can be measured in this way for a few redshifts. The values of b_1 and b_2 also contain very important information about the formation of galaxies.

With this method, Verde et al. (2002) measured the galaxy bias parameters using the observational data of 2dF Galaxy Redshift Survey (2dFGRS). They found that the linear bias factor b_1 is consistent with unity and the quadratic bias parameter b_2 is consistent with zero. Though the error bars of their measurements are also large, the results may still indicate that galaxies follow the distribution of dark matter. The range of scales assumed, however, was in the quasilinear and nonlinear regime ($0.1 < k < 0.5 h\text{Mpc}^{-1}$). On these scales, the second-order perturbation theory is already not accurate enough to predict the dark matter bispectrum, and even the bias expansion (Equation (4)) may have already broken down, as we will show below.

Considering the potential applications of this method to constrain the cosmological parameters (e.g., the amplitude of the dark matter density distribution, the equation of state of dark energy) from the measurement of b_1 , and to constrain theories of galaxy formation from measuring b_1 and b_2 , it is important to test whether and on which scale this method can produce an unbiased measurement of b_1 and b_2 . Because the bias factors are generally dependent on the scale k (against the assumption of scale-invariant b_1 and b_2), we need to check the range

TABLE 1
SIMULATION PARAMETERS

boxsize($h^{-1}\text{Mpc}$)	particles	realizations	m_{particle}
600	1024^3	3	$1.5 \times 10^{10} h^{-1} M_\odot$
1200	1024^3	4	$1.2 \times 10^{11} h^{-1} M_\odot$

of validity of Equation (4) and at the same time, we have to make sure whether it is consistent with Equation (1). We should keep in mind that for this method to be valid, the prediction of Q_m must be accurate (i.e., PT2 must be precise on large scales) and the number density of galaxies can be expanded as in Equations (3) and (4).

In our companion paper (Guo & Jing 2009), we have studied the accuracy of PT2 for the bispectrum of dark matter and we found that the PT2 prediction is not very accurate even on scales $k \approx 0.1 h\text{Mpc}^{-1}$, and high-order loop corrections are needed (e.g., Scoccimarro et al. 1998; Bernardeau et al. 2008). In the current paper, we will focus on the second point, i.e., on which scale δ_g can be expanded as in Equation (3). We generate a set of catalogs of mock galaxies from a semi-analytical model of galaxy formation. Then we measure b_1 and b_2 from the galaxy reduced bispectrum. The obtained linear bias factor b_1 is compared with the expected value determined by the ratio of power spectra (Equation (1)) in the numerical simulations. We will also demonstrate that an accurate prediction of the dark matter bispectrum is necessary for obtaining correct bias factors. We constrain our discussion only in the real space (relative to the redshift space) to avoid the complicated observational effects.

The paper is constructed as follows. We describe our simulations and galaxy mock catalogs in Section 2. The accuracy of determining the galaxy bias factors using bispectrum is displayed in Section 3. We use the halo model to study the influence of different components in Section 4. We summarize our results in Section 5.

2. N-BODY SIMULATIONS

The cosmology considered here is a canonical spatially flat cold dark matter model with the density parameter $\Omega_m = 0.268$, the cosmological constant $\Omega_\Lambda = 0.732$, the Hubble constant $h = 0.71$, and the baryon density parameter $\Omega_b = 0.045$. The primordial density field is assumed to be Gaussian with a scale-invariant power spectrum $\propto k$. For the linear power spectrum, we generate it with the CMBfast code (Seljak & Zaldarriaga 1996), and the normalization is set to $\sigma_8 = 0.85$, where σ_8 is the present linear rms density fluctuation within a sphere of radius $8 h^{-1}\text{Mpc}$.

We use an upgraded version of the Particle-Particle-Particle-Mesh (P^3M) code of Jing & Suto (1998, 2002) to simulate structure formation in the universe. The code has now incorporated the multiple level P^3M gravity solver for high-density regions (Jing & Suto 2000). In order to have a large mass resolution range, we run a total of 7 simulations with 1024^3 particles in different simulation boxes, which we hereafter denote by $L600$ and $L1200$ by different box sizes (Table 1) (Jing et al. 2007). The simulations were run on an SGI Altix 350 with 16 processors with OPENMP parallelization in Shanghai Astronomical Observatory. Dark matter halos are identified using the standard Friends-of-Friends (FOF) algo-

gorithm with a linking length b equal to 0.2 times the mean particle separation. Unbound particles (with positive binding energy) are excluded to avoid contamination. The different resolutions of the simulations enable us to check the consistency among the results from simulations of different L_{box} , as well as to investigate the behavior of bispectrum over a large dynamical range. Here, we choose the Fourier space bin scheme as $\Delta \log_{10}(k) = 0.1$ for $k < 0.1 h\text{Mpc}^{-1}$ and 0.05 for $k > 0.1 h\text{Mpc}^{-1}$ when measuring the bispectrum.

For the galaxy samples, we build our catalogs on the semi-analytical model of Croton et al. (2006). They have generated the galaxy distribution in the Millennium Simulation with the box size $L_{box} = 500 h^{-1}\text{Mpc}$ on a side (Springel et al. 2005). The cosmological parameters used in Croton et al. (2006) ($\Omega_m = 0.25$, $\Omega_\Lambda = 0.75$, $\Omega_b = 0.045$, $h = 0.73$, $\sigma_8 = 0.9$) are not exactly the same as ours. But the slight difference in the parameters is not the focus in this paper, since an approximate relation connecting galaxies to dark matter is sufficient here. For each dark matter halo in our simulations, we randomly choose a corresponding galaxy host halo of the same mass from the galaxy catalog of Croton et al. (2006). One thing to note is that the virial masses of the halos in Croton et al. (2006) are defined by the spherical overdensity approach, which makes their final halo masses about 1.5 times smaller than those of our corresponding FOF halos. We adjust the masses of Croton et al. (2006) halos, so they would match our halo definitions. After the adjustment, we put those galaxies of the host halos of Croton et al. (2006) into our corresponding dark matter halos, while preserving the same relative positions to the halo centers. Finally, we obtain the corresponding distributions of galaxies in our simulations, as well as their properties, such as the luminosity and velocity. We use the r-band magnitude for the luminosity of galaxies, M_r , which is defined to be $M_r = M_{abs} + 5 \lg h$, that is, the absolute magnitude M_{abs} when $h = 1$.

We show in the top panel of Figure 1 the probability distribution of the virial mass m of our simulation dark matter halos. $L1200$ has more massive halos than $L600$, thus $L1200$ can be used to investigate the distribution of more luminous galaxies while $L600$ for ordinary galaxies with moderate luminosity. The sharp cut for each L_{box} represents the minimum mass of the dark matter halos that consist of at least 10 particles in our definition. The host halo mass distributions of the central and satellite galaxies in the galaxy catalog of Croton et al. (2006) are also shown in the middle and bottom panels of Figure 1, respectively. We divide the galaxy samples into subsamples of different luminosity, and the probability distribution of host halo masses are shown as the different lines in the figure.

To avoid incompleteness, the available galaxy subsamples are actually limited for each L_{box} simulation. As it is shown in Figure 1, we can use all those galaxies with $M_r < -20$ for $L600$ (However, the most luminous galaxies with $M_r < -23$ are not abundant in $L600$, which will cause large fluctuations in their bispectrum statistics. That is why we do not consider this luminosity subsample for $L600$). For $L1200$, because dark matter halos have high mass of $m > 10^{12} h^{-1}M_\odot$, only those galaxies of $M_r < -22$ will be analyzed.

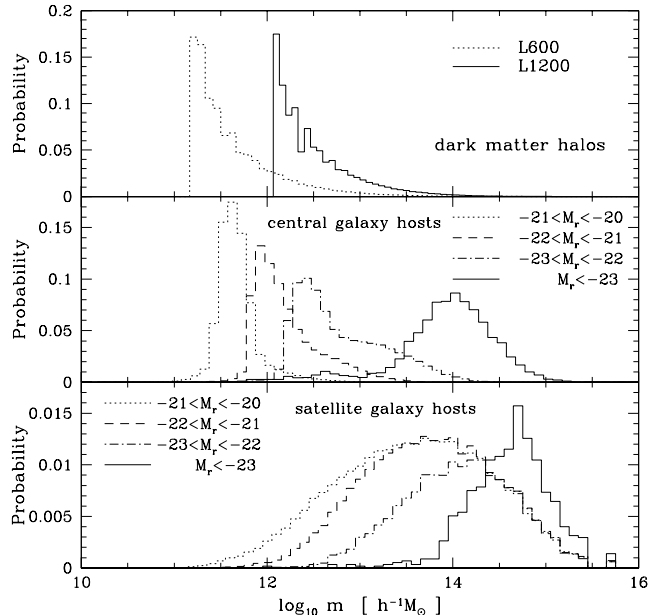


FIG. 1.— Probability distribution of the virial mass m of the dark matter halos in our simulations (Top). The host halo mass distributions of the central and satellite galaxies in the galaxy catalog of Croton et al. (2006) are also shown in the middle and bottom panels.

3. GALAXY BIASING

To obtain the galaxy bias factors by fitting Equation (4), one needs an accurate error estimation for the galaxy bispectrum Q_g . Since we do not have enough independent Fourier space k modes on large scales of $k < 0.1 h\text{Mpc}^{-1}$ (finite-volume effect), and the number of realizations for each L_{box} simulation are also limited, the large fluctuations among different realizations on large scales would prevent us from making an accurate error estimation of Q_g . So we use the Gaussian uncertainties, instead of the simulation fluctuations, as the errors for Q_g .

The uncertainty of bispectrum for a Gaussian density field reads (e.g., Fry & Gaztañaga 1993; Scoccimarro et al. 1998, 2004; Sefusatti & Komatsu 2007)

$$\langle \Delta B_g^2 \rangle = \frac{1}{N_{123}} P_{tot}(k_1) P_{tot}(k_2) P_{tot}(k_3) \quad (7)$$

$$P_{tot}(k) = P_g(k) + \frac{1}{N_p}, \quad (8)$$

where N_{123} is the number of independent triangle configuration modes in the Fourier space, and $P_{tot}(k)$ includes the shot noise in the galaxy power spectrum for the case of N_p objects. Although we measure N_{123} directly from the simulations, it can be estimated theoretically as (Sefusatti & Komatsu 2007)

$$N_{123} \approx \frac{8\pi^2}{s_{123} k_f^6} k_1 k_2 k_3 \Delta k_1 \Delta k_2 \Delta k_3, \quad (9)$$

where $k_f = 2\pi/L_{box}$ and $s_{123} = 6, 2, 1$ for equilateral, isosceles and general triangles. By assuming that the variance of bispectrum dominates over that of the power spectrum, variance of the reduced bispectrum is then given by,

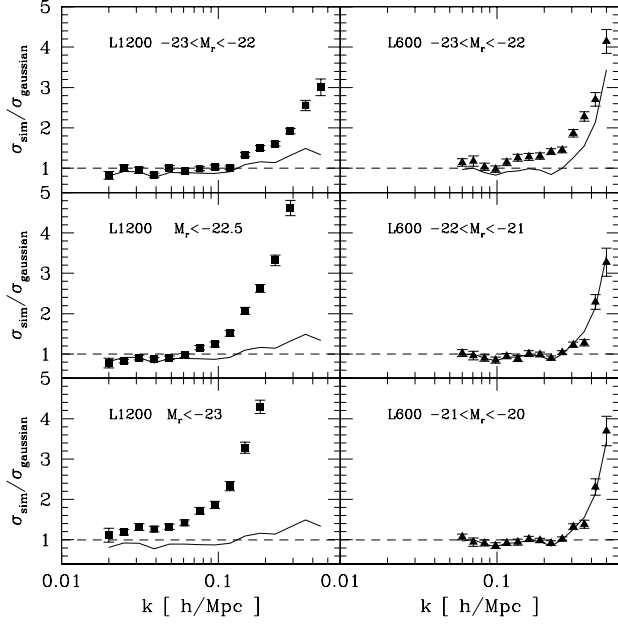


FIG. 2.— Ratios of the reduced bispectrum errors measured from simulations to the errors based on the Gaussian field assumption. Those points are for galaxies of different luminosity (as shown in each panel), while the solid lines represent the ratios for dark matter.

$$\langle \Delta Q_g^2 \rangle = \frac{\langle \Delta B_g^2 \rangle}{[P_g(k_1)P_g(k_2) + cyc]^2}. \quad (10)$$

The fluctuation of Q_g is thus directly determined by the number of independent triangle modes, N_{123} , which are actually related to the simulation box size, L_{box} . The larger box simulation has higher precision in the determination of bispectrum on large scales, especially for $k < 0.1 h\text{Mpc}^{-1}$. In addition to the considerable fluctuations, the finite-volume effect is also significant for the bispectrum on large scales. Because the bispectrum essentially reflects the influence of the gravitational instability, the existence of large-scale structures, such as filaments, will significantly affect the final bispectrum estimation (e.g., Sefusatti & Scoccimarro 2005). Overall, large L_{box} simulations are essential if we want to determine the bispectrum on such large scales with unerring accuracy, as we have processed in this paper.

Figure 2 shows the ratios between the errors on the mean of Q averaged over the realizations and the corresponding uncertainties based on the Gaussian assumption. The ratios for galaxies of different luminosity (symbols) are compared with those ratios for dark matter (solid lines) for both $L1200$ and $L600$. Given that triangles with a side in common will correlate with each other, we alleviate this problem by defining the scale k in Figure 2 to be the longest side of the triangle and by including all the triangle configurations in each k bin. The remaining correlations are ignored. So, each data point in Figure 2 represents the mean of all the triangle configurations whose longest sides are in the same k bin, and the $1 - \sigma$ error shown is the fluctuation among the different triangle configurations. The small discrepancies of dark matter ratios between $L1200$ and $L600$ are caused by the different simulation resolutions, with $L1200$ more

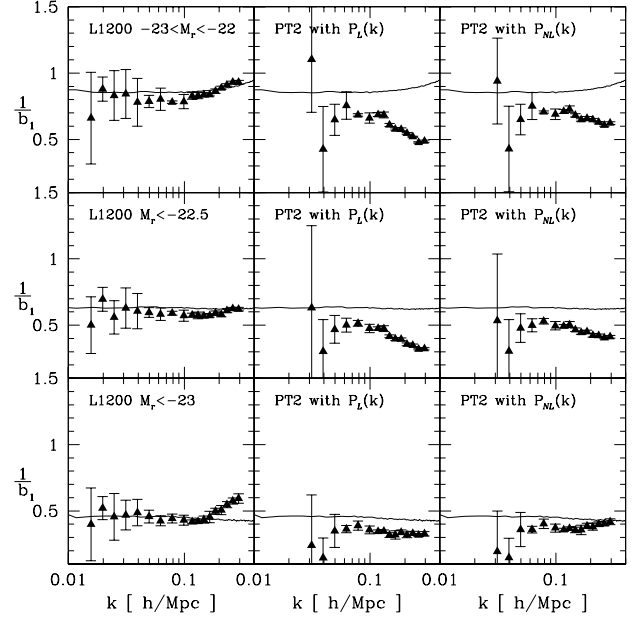


FIG. 3.— χ^2 fitting results of Equation (4) for the linear bias factor $b_1(k)$ in the galaxy samples of $L1200$. The left panels show the fittings with Q_m determined from $L1200$ simulations. In the middle panels, Q_m is estimated with PT2 using the linear power spectrum $P_L(k)$ in Equation (2) and Equation (5). In the right panels, Q_m is also estimated with PT2, but the nonlinear power spectrum $P_{NL}(k)$ estimated directly from the simulation is used for the PT2 predictions. The solid lines denote the expected value derived from the power spectrum ratios in Equation (1). The scale k is defined as the maximum value of the triangle sides (k_1, k_2, k_3).

reliable on large scales and $L600$ on small scales. As for galaxies of $M_r > -23$, the reduced bispectrum errors can be well described by the Gaussian errors on large scales of $k < 0.1 h\text{Mpc}^{-1}$. The galaxies have similar error ratios to those of dark matter, implying that the deviation of the bispectrum error from the Gaussian field error is slim in the linear clustering regime. For the galaxy samples of $M_r < -23$, the simulation variances deviate rapidly from the Gaussian uncertainties even on large scales. This is because these galaxies are highly biased, and the non-Gaussianity already plays an important role in determining $\langle \Delta Q_g^2 \rangle$ for such luminous galaxies. Since we are interested in the behavior of the bias factors at $k < 0.2 h\text{Mpc}^{-1}$, we will use Equation (10) to estimate the errors for the galaxy reduced bispectrum.

In Figure 3 ($L1200$) and Figure 4 ($L600$), we show the χ^2 fitting results of Equation (4) for the linear bias factor $b_1(k)$. The left panels show the fitting results with Q_m measured from simulations, and the middle panels show the results with Q_m determined by PT2. As in observations, we also use the nonlinear power spectrum $P_{NL}(k)$ in Equations (2) and (5) for the PT2 estimation of Q_m , and the results are shown in the right panels. The solid lines denote the predictions derived from the power spectrum ratios as in Equation (1). Again, the scale k in the figures is defined as the maximum triangle size of (k_1, k_2, k_3). And for each k bin, we have included all types of triangle shapes to make the fittings. The jump in the errors of $L600$ at $0.1 h\text{Mpc}^{-1}$ is caused by our change of Fourier space bin scheme at this scale.

In the left panels, the bias factor $b_1(k)$ determined

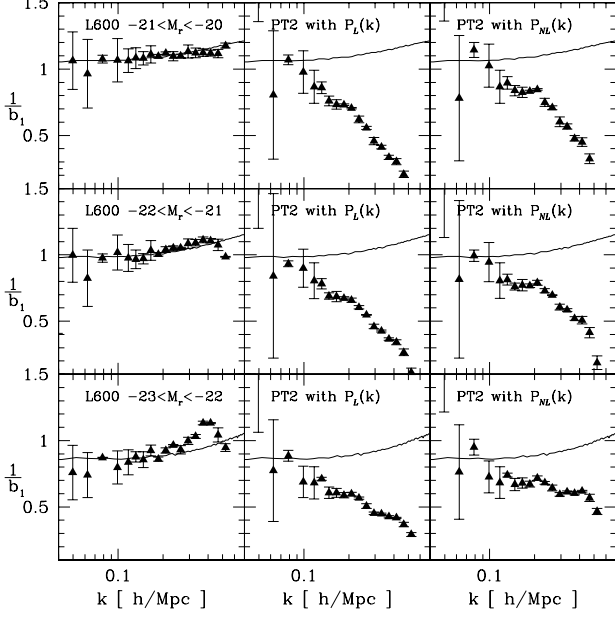


FIG. 4.— Same as Figure 3, but for $L600$ galaxy samples.

by Equation (4) is well consistent with that of the power spectrum ratio (Equation(1)) on large scales of $k < 0.15 h\text{Mpc}^{-1}$. This indicates that $b_1(k)$ can be reconstructed from bispectrum observations of galaxies without significant systematic bias. However, when Q_m is calculated from PT2 (the middle panels), the fitted $b_1(k)$ are overestimated on most scales except for the largest one of $k \sim 0.03 h\text{Mpc}^{-1}$ where the fluctuation is dramatic. The main reason is that PT2 overestimates Q_m for collinear configurations ($\alpha \equiv \arccos(\mathbf{k}_1 \cdot \mathbf{k}_2)/k_1 k_2 = 0$ and π) and underestimates for triangles of $\alpha \approx 0.6\pi$ even on large scales of $k \approx 0.1 h\text{Mpc}^{-1}$ (Guo & Jing 2009). Using the nonlinear power spectrum for the PT2 prediction of Q_m does not improve the fitting results, as shown by the right panels. Our results clearly show that it is necessary to have an accurate estimation of the dark matter bispectrum if Equation (4) is used to get the galaxy bias factors.

When the scale goes down to $k > 0.15 h\text{Mpc}^{-1}$, the nonlinear effects become important. The linear bias $b_1(k)$ does not keep a constant on these small scales. Then the premise of the fittings that b_1 and b_2 both are scale-invariant in Equation (4) breaks down. We would expect that these bias factors from the power spectrum ratios and from the bispectrum fittings will be different, though we note that they agree well on scales down to $k = 0.4 h\text{Mpc}^{-1}$ for galaxy samples of $M_r > -23$, which could be a coincidence. As PT2 breaks down for the prediction of dark matter bispectrum even on scales slightly larger than that of $k = 0.1 h\text{Mpc}^{-1}$, our results show the expansion of the galaxy density fields in Equation (3) is valid on the smaller scales ($k = 0.15 h\text{Mpc}^{-1}$).

To verify the conclusions above, we also show the scale dependence of b_2/b_1^2 in Figure 5 ($L1200$) and Figure 6 ($L600$). We see that b_2/b_1^2 is nearly a constant on large scales of $k < 0.15 h\text{Mpc}^{-1}$. With the scale independence of b_1 on these scales, we infer that the nonlinear bias b_2 is

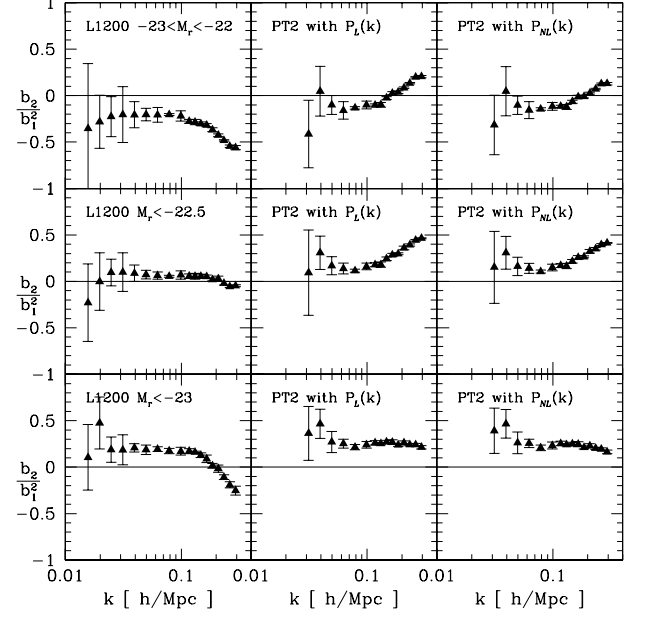


FIG. 5.— Same as Figure 3, but for the scale dependence of b_2/b_1^2 . The solid lines show the case of a vanishing nonlinear bias factor b_2 for comparison. Since the error bars are much too large for $k < 0.03 h\text{Mpc}^{-1}$ in the middle and right panels, we do not show those data points here.

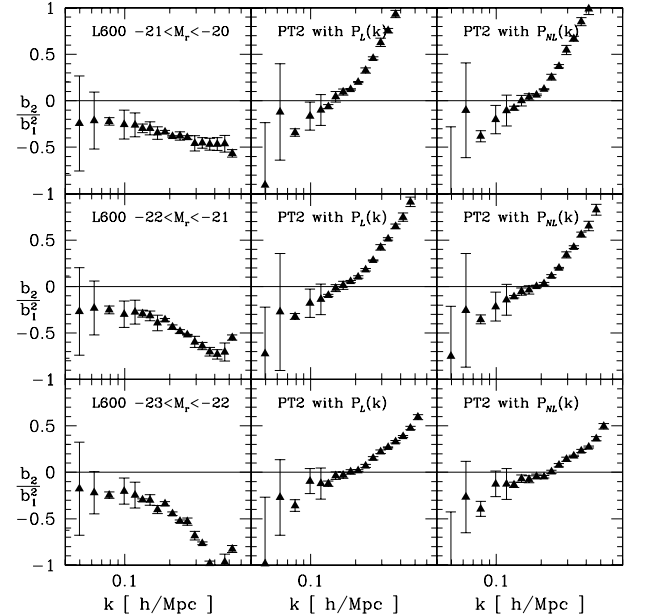


FIG. 6.— Same as Figure 5, but for $L600$ simulations.

also scale invariant for small k . It again confirms the feasibility of deriving b_1 and b_2 from Equation (4) through direct χ^2 fittings. But b_2 deviates from such constancy as the scale goes to the nonlinear scales, similar to the case of the linear bias b_1 . In general, the nonlinear bias b_2 is nonvanishing on large scales and plays an important role in the determination of the linear bias factor b_1 when using Equation (4). It is interesting to note that the most luminous samples have positive values of

b_2 ($b_2 \approx 1.2$ for $M_r < -23$ and $b_2 \approx 0.3$ for $M_r < -22.5$) on large scales, but fainter samples have negative values of b_2 (e.g., $b_2 \approx -0.2$ for $-21 < M_r < -20$ and $b_2 \approx -0.3$ for $-23 < M_r < -22$). We note that the values of b_2/b_1^2 for galaxy samples with $M_r > -22.5$ are nearly the same with $b_2/b_1^2 = -0.2$ at $k < 0.1 h\text{Mpc}^{-1}$, which might be a coincidence for this particular semi-analytical model of galaxy formation. The general behavior that b_2 increases with the luminosity at the high luminosity end, and decreases with increasing luminosity at fainter luminosity, is consistent with the change of nonlinear halo bias $b_2(m)$ with the dark matter halo mass m (Mo, Jing & White 1997).

The middle and right panels of Figure 5 and Figure 6 clearly demonstrate the failure of the fittings for the bias factors when using PT2 to calculate Q_m . (Since the error bars are much too large for $k < 0.03 h\text{Mpc}^{-1}$, we do not show those data points here.) Thus PT2 is actually not a good estimator for the reduced dark matter bispectrum Q_m when we want to use it to fit the bias factors with Equation (4). Verde et al. (2002) used PT2 as the preferred choice for the estimation of Q_m and they determine the bias factors for $k = 0.1 \sim 0.5 h\text{Mpc}^{-1}$. As we showed above, on these scales, the PT2 is not accurate enough (see Guo & Jing 2009) and the fitting results of the bias factors are biased even if the measurement of Q_g from galaxy surveys is accurate.

4. AN ATTEMPT TO STUDY THE BISPECTRUM AT QUASILINEAR REGIME WITH THE HALO OCCUPATION MODEL

Since the PT2 as well as the Taylor expansion breaks down quickly on quasilinear scales ($k > 0.1 h\text{Mpc}^{-1}$), we want to explore if the halo occupation distribution (HOD) model of galaxies (e.g., Jing et al. 1998; Berlind & Weinberg 2002; Yang, Mo, & van den Bosch 2003; Zheng et al. 2005) can extend the theoretical modeling to quasilinear and even nonlinear scales. The HOD model has been used to predict the bispectrum of galaxies in numerical simulations (Jing & Börner 1998; Jing & Börner 2004; Nichol et al. 2006; Kulkarni et al. 2007; Nishimichi et al. 2007; Marín et al. 2008) and in analytical modeling (Scoccimarro et al. 2001; Takada & Jain 2003; Wang et al. 2004). In this section, we check if the bispectra of galaxies on quasilinear scales can be modeled with the latter method.

The necessary halo model ingredients are described as follows. The dark matter halos are defined as objects with a mean density Δ_{vir} times that of the background universe (Bryan & Norman 1998) where $\Delta_{vir} \approx 361$ for our cosmology parameters, and their density distributions follow the Navarro–Frenk–White (NFW) profile (Navarro, Frenk, & White 1997). The concentration parameter $c(m)$ of the halos is given by the relation $c(m) = c_0(m/m_*)^\beta$, where $c_0 = 9$, $\beta = -0.13$, and $m_* = 4.8 \times 10^{12} h^{-1} M_\odot$ is the nonlinear mass scale (Bullock et al. 2001). We also use the same linear power spectrum as that used for generating the initial condition for the simulations. For the halo mass function (MF) $n(m)$, we consider the analytical models of Press & Schechter (1974) (PS) and Sheth & Tormen (1999) (ST). For the halo bias parameters $b_i(m)$ ($i = 1, 2$), we use the corresponding results of Mo, Jing & White (1997) and Sheth & Tormen (1999) for PS and ST mass functions,

respectively. The last ingredient of the model are the different moments of the galaxy distribution within the parent halos, i.e., the halo occupation number $\langle N_g(m) \rangle$, the second moment $\langle N_g(N_g - 1) \rangle$ and the third moment $\langle N_g(N_g - 1)(N_g - 2) \rangle$. They are derived directly from the galaxy mock catalogs, and are inserted into the integrals of the halo model with interpolations of the simulation data points.

Following Scoccimarro et al. (2001), the galaxy power spectrum and bispectrum are given by

$$P_g(k) = [G_{11}(k)]^2 P_L(k) + G_{02}(k, k) \quad (11)$$

$$\begin{aligned} B_g(k_1, k_2, k_3) = & G_{11}(k_1)G_{11}(k_2)G_{11}(k_3)B_{PT} \\ & + [G_{11}(k_1)G_{11}(k_2)G_{21}(k_3)P_L(k_1)P_L(k_2) + \text{cyc}] \\ & + [G_{11}(k_1)G_{12}(k_2, k_3)P_L(k_1) + \text{cyc}] \\ & + G_{03}(k_1, k_2, k_3), \end{aligned} \quad (12)$$

where

$$\begin{aligned} G_{ij}(k_1, \dots, k_j) \equiv & \int dmn(m) \frac{\langle N_g^j(m) \rangle}{\bar{n}_g^j} b_i(m) \\ & \times [u(k_1|m) \dots u(k_j|m)] \end{aligned} \quad (13)$$

and $b_0 \equiv 1$. $\langle N_g^j(m) \rangle$ represents the different moments of the galaxy distribution mentioned above, $u(k|m)$ is the normalized Fourier transform of the dark matter halo density profile $\rho(r|m)$ truncated at the virial radius, and \bar{n}_g denotes the mean number density of galaxies,

$$\bar{n}_g = \int dmn(m) \langle N_g(m) \rangle. \quad (14)$$

We note that $\langle N_g^j(m) \rangle$ can be further decomposed into the central and satellite galaxy components and for the central galaxies, $u(k|m) = 1$. The galaxy reduced bispectrum Q_g is then defined as

$$Q_g(k_1, k_2, k_3) = \frac{B_g(k_1, k_2, k_3)}{P_g(k_1)P_g(k_2) + \text{cyc}}. \quad (15)$$

In Figure 7, we show the ratio of the galaxy power spectrum $P_g(k)$ to the linear dark matter power spectrum $P_L(k)$ only for the galaxy samples of $-23 < M_r < -22$. The points denote the results of the simulations (the shot-noise effect has been corrected), and the different lines represent the halo model predictions for different halo mass functions. Interestingly, the model predictions agree very well with themselves on large scales, indicating that the predictions on scales larger than that of $k = 0.2 h\text{Mpc}^{-1}$ are robust against the changes of the mass function and corresponding bias functions. However, the halo model predictions are larger than those of the simulations by about 16% (from $0.03 h\text{Mpc}^{-1}$ to $0.15 h\text{Mpc}^{-1}$) on large scales. The wiggles shown on large scales of the simulation results are caused by the Baryonic Acoustic Oscillations (BAO). In the halo model configurations, BAO is indeed embedded in the linear power spectrum $P_L(k)$. Then the ratio $P_g(k)/P_L(k)$ for the halo model will display no trace of oscillation on large scales, as shown in Figure 7. Since galaxies as well as the underlying dark matter evolve in a nonlinear pattern, the resulting nonlinear power spectrum $P_g(k)$ would, however,

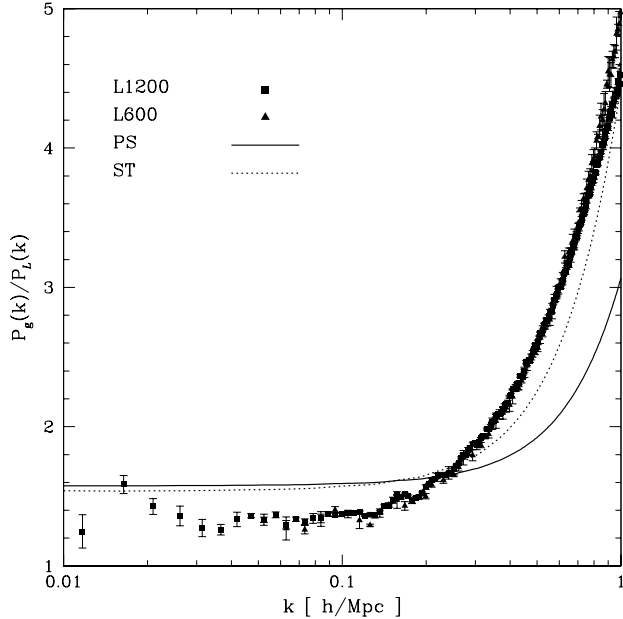


FIG. 7.— Ratio of the galaxy power spectrum $P_g(k)$ to the linear dark matter power spectrum $P_L(k)$ for the galaxy samples of $-23 < M_r < -22$. The points denote the results from different L_{box} simulations, and the lines represent the analytical predictions of the halo models for different halo mass functions.

still remain some features of BAO, but the nonlinear processes do suppress the BAO features. (Because $P_L(k)$ appears in the denominator of the ratio, the peaks shown in Figure 7 should actually correspond to the troughs in the linear theory.) The differences of the simulation results between $L1200$ and $L600$ at $k > 0.7 \, h\text{Mpc}^{-1}$ are due to the limited resolution of $L1200$.

In halo model, $P_g(k)$ consists of two components, the 1-halo and 2-halo terms. On small scales, the 1-halo term which is actually dominant has no dependence on the halo bias parameters. So the differences of the halo models on the small scales mostly come from the choices of different MFs. Our results do favor the ST MF over the PS MF as expected. On large scales, the dominant component is the 2-halo term and the linear halo bias factor $b_1(m)$ influences the final predictions. The poor agreement between the simulation results and the predictions of the PS and ST models, implies that the MFs and the halo bias functions derived from the peak-background split assumption, might not be fully consistent with the simulation results. And the similar predictions between PS and ST models on large scales also suggest that the inconsistency is probably due to intrinsic defects of the halo model configurations. The deficiency of halo models is also revealed by the fact that the BAO wiggles on large scales can not be well described by the halo models. Here, we do not consider the exclusion effect and the halo boundary effect (see e.g., Takada & Jain 2003; Smith et al. 2006), which are important only on the quasilinear and nonlinear regimes.

In Figure 8, we show the halo model predictions of the galaxy reduced bispectrum $Q_g(k, u, \alpha)$ where k (referring to k_1 in $Q_g(k_1, k_2, k_3)$) describes the size of triangle, $u \equiv k_2/k_1$, and $\alpha \equiv \arccos(\mathbf{k}_1 \cdot \mathbf{k}_2)/k_1 k_2$. The square and triangle open points stand for the simulation results of

$L1200$ and $L600$, respectively. The solid and dotted lines represent the halo model predictions for the PS and ST MFs, respectively. As in Figure 7, the galaxies analyzed are in the luminosity range of $-23 < M_r < -22$. We also show for comparison the dark matter reduced bispectrum Q_m (solid symbols) and PT2 predictions (dashed lines). At first glance, the linear relation of Equation (4) seems to be true, confirming our conclusions above.

On all the scales, the PS model seems to fit the simulations better, while the ST model predicts a larger Q_g . The difference in the model predictions might reflect the fact that the ST MF has more massive halos than the PS MF. On large scales of $k < 0.05 \, h\text{Mpc}^{-1}$, the predictions of PS model are consistent with the simulation results fairly well. But the model predictions for the ST MF are still larger than those of the simulations except for the case of $k = 0.03 \, h\text{Mpc}^{-1}$, where the fluctuation among the simulation realizations is dramatic.

On the intermediate scales of $0.06 \, h\text{Mpc}^{-1} \sim 0.1 \, h\text{Mpc}^{-1}$, the PS model agrees with the simulations for isosceles triangle configurations but is larger for the collinear configurations while the ST model predictions are always larger than the simulation results. On smaller scales, Q_g from simulations shows a flattening trend around the isosceles triangle configurations, as in the bottom panels of Figure 8. But such a feature is not seen so evidently in the halo models.

As in the case of galaxy power spectrum, the halo model is still not accurate enough to fulfil the requirement of precision studies of the galaxy bispectrum. Since Q_g is the ratio of bispectrum B_g to a sum of power spectrum products, any better agreement achieved with the PS MF is more likely to be a coincidence, considering the poor agreement in the $P_g(k)$ predictions. Therefore, the framework of the halo model, including its important ingredients, needs to be further digested in future studies.

5. CONCLUSIONS

We use a set of numerical N -body simulations to study the large scale behavior of the galaxy bias parameters with the bispectrum method. We first determine the dark matter distribution from our simulations and then construct our mock galaxy catalogs from the semi-analytical model of Croton et al. (2006). The galaxy bias parameters b_1 and b_2 can be simply obtained by fitting the relation of Equation (4) given the knowledge of the dark matter and galaxy bispectra.

We find that on large scales down to $k \approx 0.15 \, h\text{Mpc}^{-1}$, the bias factors b_1 and b_2 are nearly constant. More importantly, b_1 obtained from the bispectrum method is consistent with that from the power spectrum ratio (Equation (1)), indicating that the linear bias factor b_1 can be obtained from the distribution of galaxies. Also in general, the nonlinear bias b_2 is not zero; it is of a negative value for galaxies of typical luminosity, and increases to a positive value for the most luminous galaxies. On scales of $k > 0.15 \, h\text{Mpc}^{-1}$, the bias factors rapidly deviate from the constancy shown on large scales. This is because the nonlinear effects become important on these quasilinear and nonlinear regimes. On these scales, the simple relation between Q_g and Q_m in Equation (4) or the assumption that b_1 and b_2 are constant is not valid. It is therefore not effective to use this relation to obtain

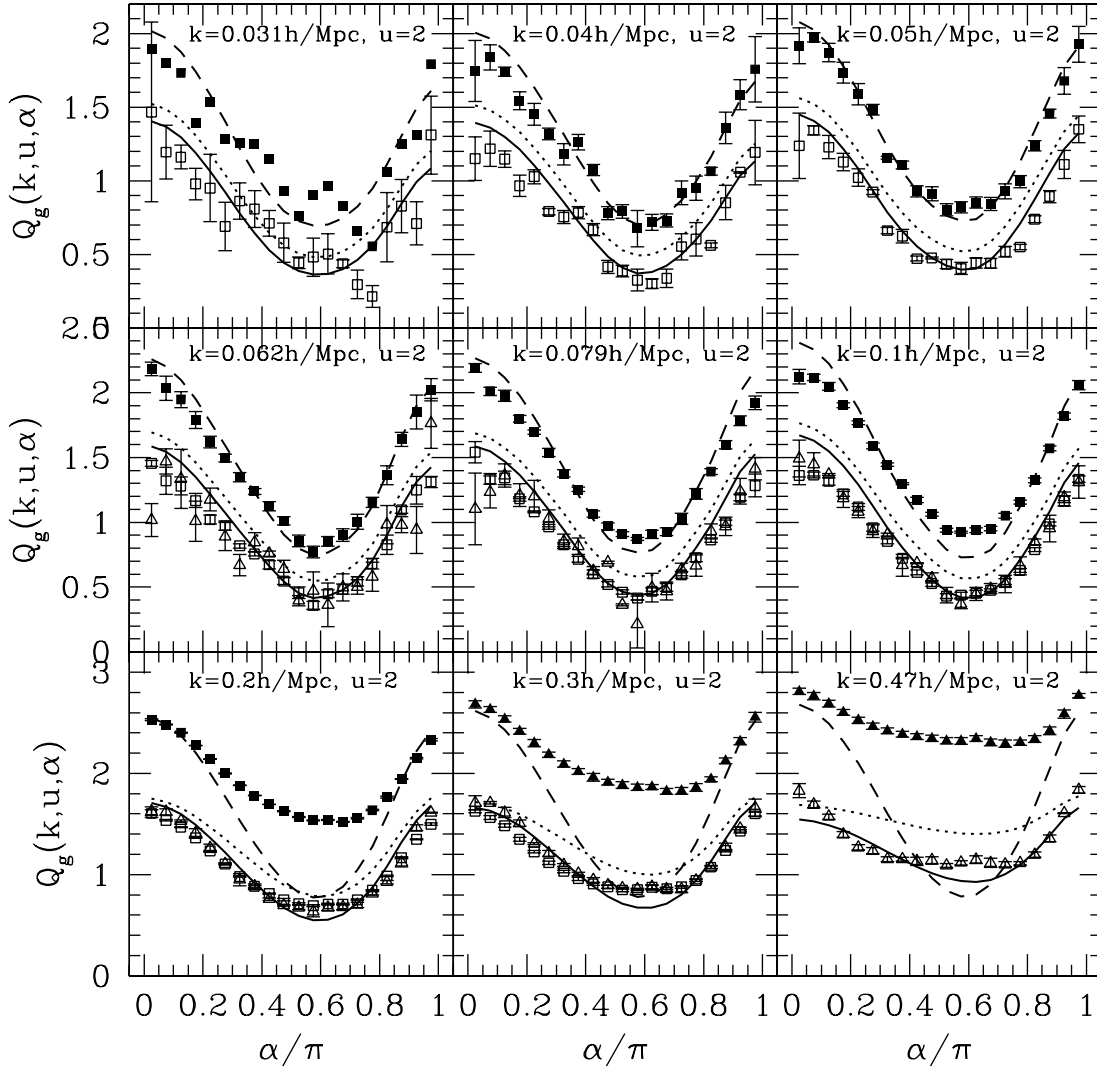


FIG. 8.— Scale and shape dependence of the galaxy bispectrum Q_g from the analytical predictions of halo models, compared with the results from the simulations for the galaxy samples of $-23 < M_r < -22$. The square and triangle open points stand for the results of $L1200$ and $L600$, respectively. The solid and dotted lines represent the model predictions for PS and ST MFs, respectively. We also show for comparison the dark matter reduced bispectrum Q_m (solid symbols) and PT2 predictions (dashed lines).

the bias factors on small scales.

We also try PT2 to estimate the dark matter bispectrum in the bias Equation (4). But the poor agreement with the known linear bias factor shows that it is very important to accurately estimate the dark matter bispectrum when using Equation (4). This indicates that PT2 is still not accurate enough for the dark matter bispectrum estimation even on fairly large scales. Thus, it again implies that higher-order corrections, such as the one-loop correction (Scoccimarro & Frieman 1996) in the perturbation theory, are necessary for more precise estimation of the bispectrum in the further studies.

Because of the simple structure of the halo model method, we also incorporate HOD from our mock galaxy catalogs to model the galaxy power spectrum and bispectrum, as shown in Figure 7 and Figure 8. Overall,

the analytical halo models are not accurate enough to describe the power spectrum and bispectrum of galaxies on the requirement of current precision studies. More work is needed to improve the analytical halo model.

We thank the anonymous referee for helpful suggestions. This work is supported by NSFC (10533030, 10821302, 10873028, 10878001), by the Knowledge Innovation Program of CAS (no. KJCX2-YW-T05), and by the 973 Program (no.2007CB815402). The Millennium Run simulation used in this paper was carried out by the Virgo Supercomputing Consortium at the Computing Centre of the Max-Planck Society in Garching. The semi-analytic galaxy catalogue is publicly available at <http://www.mpa-garching.mpg.de/galform/agnpaper>.

REFERENCES

- Bardeen, J. M., Bond, J. R., Kaiser, N., & Szalay, A. S. 1986, ApJ, 304, 15
- Berlind, A. A. & Weinberg, D. H. 2002, ApJ, 575, 587

- Bernardeu, F., Colombi, S., Gaztañaga, E., & Scoccimarro, R., 2002, *Phys. Rep.*, 367, 1
- Bernardeu, F., Crocce, M., & Scoccimarro, R. 2008, *Phys. Rev. D*, 78, 103521
- Börner, G., Deng, Z. G., Xia, X. Y., & Zhou, Y. Y. 1991, *Ap&SS*, 180, 47
- Bryan, G., Norman, M. 1998, *ApJ*, 495, 80
- Bullock, J. S., Kolatt, T. S., Sigad, Y., Somerville, R. S., Klypin, A. A., Primack, J. R., Dekel, A. 2001, *MNRAS*, 321, 559
- Coles, P. 1993, *MNRAS*, 262, 1065
- Croton D. J., Springel V., White S. D. M., et al., 2006, *MNRAS*, 365, 11
- Davis, M., Efstathiou, G., Frenk, C. S., & White, S. D. M. 1985, *ApJ*, 292, 371
- Fry, J. N. 1984, *ApJ*, 279, 499
- Fry, J. N. 1994, *Phys. Rev. Lett.*, 73, 215
- Fry, J. N., Gaztañaga, E. 1993, *ApJ*, 413, 447
- Gaztanaga, E., & Frieman, J. A. 1994, *ApJ*, 437, L13
- Guo, H. & Jing, Y. P. 2009, *ApJ*, 698, 479
- Jing, Y. P. & Börner, G. 1998, *ApJ*, 503, 37
- Jing, Y. P., Börner, G., & Suto, Y. 2002, *ApJ*, 564, 15
- Jing, Y. P., & Börner, G. 2004, *ApJ*, 607, 140
- Jing, Y. P., Mo, H. J., & Börner, G. 1998, *ApJ*, 494, 1
- Jing, Y. P., & Suto, Y. 1998, *ApJ*, 494, L5
- Jing, Y. P., & Suto, Y. 2000, *ApJ*, 529, L69
- Jing, Y. P., & Suto, Y. 2002, *ApJ*, 574, 538
- Jing, Y. P., Suto, Y., & Mo, H. J. 2007, *ApJ*, 657, 664
- Kaiser, N. 1984, *ApJ*, 284, L9
- Kulkarni, G. V., Nichol, R. C., Sheth, R. K., Seo, H. J., Eisenstein, D. J. & Gray, A. 2007, *MNRAS*, 378, 1196
- Li, C., Kauffmann, G., Jing, Y. P., White, S. D. M., Börner, G., & Cheng, F. Z. 2006, *MNRAS*, 368, 21
- Marín, F. A., Wechsler, R. H., Frieman, J. A., & Nichol, R. C. 2008, *ApJ*, 672, 849
- Matarrese, S., Verde, L., & Heavens, A. F. 1997, *MNRAS*, 290, 651
- Meneux, B., et al. 2008, *A&A*, 478, 299
- Mo, H. J., Jing, Y. P., & White, S. D. M., 1997, *MNRAS*, 290, 651
- Navarro, J. F., Frenk, C. S., & White, S. D. M. 1997, *ApJ*, 490, 493
- Nichol, R. C., et al. 2006, *MNRAS*, 368, 1507
- Nishimichi, T., Kayo, I., Hikage, C., Yahata, K., Taruya, A., Jing, Y. P., Sheth, R. K. & Suto, Y. 2007, *PASJ*, 59, 93
- Norberg, P., et al. 2002, *MNRAS*, 332, 827
- Park, C., et al. 2005, *ApJ*, 633, 11
- Press, W. H., & Schechter, P. 1974, *ApJ*, 187, 425
- Scoccimarro, R., Colombi, S., Fry, J. N., Frieman, J. A., Hivon, E., Melott, A. 1998, *ApJ*, 496, 586
- Scoccimarro, R., & Frieman, J. 1996, *ApJ*, 105, 37
- Scoccimarro, R., Sefusatti, E., & Zaldarriaga, M. 2004, *Phys. Rev. D*, 69, 103513
- Scoccimarro, R., Sheth, R. K., Hui, L., & Jain, B. 2001, *ApJ*, 546, 20
- Sefusatti, E., & Komatsu, E., 2007, *Phys. Rev. D*, 76, 083004
- Sefusatti, E., & Scoccimarro, R., 2005, *Phys. Rev. D*, 71, 063001
- Seljak, U., & Zaldarriaga, M., 1996, *ApJ*, 469, 437
- Sheth, R. K. & Tormen, G. 1999, *MNRAS*, 308, 119
- Smith, R. E., Watts, P. I. R. & Sheth, R. K. 2006, *MNRAS*, 365, 214
- Springel, V., et al. 2005, *Nature*, 435, 629
- Takada, M., & Jain, B. 2003, *MNRAS*, 340, 580
- Verde L., et al. 2002, *MNRAS*, 335, 432
- Wang, Y., Yang, X. H., Mo, H. J., van den Bosch, F. C. & Chu, Y. 2004, *MNRAS*, 353, 287
- Xia, X. Y., Deng, Z. G., & Zhou, Y. Y. 1987, *Observational Cosmology*, 124, 363
- Yang, X. H., Mo, H. J., & van den Bosch, F. C. 2003, *MNRAS*, 339, 1057
- Zehavi, I., et al. 2004, *ApJ*, 608, 16
- Zheng, Z., et al. 2005, *ApJ*, 633, 791